Int. J. High Technology Ceramics **3** (1987) 179–197

Strength Characterization of Yttria/Alumina-Doped Sintered Silicon Nitride

R. K. Govila

Ceramic Materials Department, Research Staff, Ford Motor Company,
PO Box 2053, Dearborn, Michigan 48121, USA

SUMMARY

The flexural strength of yttria/alumina-doped sintered silicon nitride (Ford Material—RM 20) was measured as a function of temperature (20 to 1400°C), applied stress and time. Flexural stress rupture testing at 800 and 1000°C indicated that the material can sustain 344 MPa and 276 MPa, respectively, without failure, for a limited time ($\leq$100 h). The RM 20 material was susceptible to both oxidation and early stages of creep deformation at temperatures above 1000°C and displayed extensive creep deformation and degradation in strength above 1300°C.

1 INTRODUCTION

Silicon nitride containing yttria, in hot-pressed and sintered forms, are currently being evaluated for use as structural components at high temperatures (> 1000°C) for gas turbines, because of high strength and good thermal shock resistance. Hot-pressed material is limited in commercial use to simple shapes like solid circular disks, and rectangular or triangular pieces like cutting tool inserts. Structural engine components like turbine stators and rotors cannot be fabricated into a net shape by conventional hot-pressing methods, and machining from hot-pressed billets is too expensive and time consuming. By contrast, sintered material offers an advantage over the hot-pressed material, since many structural components can be fabricated using commercial injection molding or slip casting techniques. Under suitable conditions (time, temperature, pressure and environment),

Int. J. High Technology Ceramics 0267-3762/87/$03·50

engine parts can be sintered to full density, provided allowance is made for sintering shrinkages. Recently, some success has been achieved in fabricating engine components to near net shape using the hipping (hot isostatic pressing) technique or process.

This study was undertaken to characterize the strength behavior of an in-house (Ford Scientific Laboratory) developed yttria/alumina-doped sintered silicon nitride (Ford material—RM 20) by evaluating the fracture strength as a function of temperature (20 to 1400°C in air); failure sites and the mode of crack propagation were examined fractographically. In addition, long term reliability and durability were characterized using flexural stress rupture testing at several temperatures.

2 MATERIAL, SPECIMEN PREPARATION AND TESTING

This material (hereafter referred as RM 20) is a sintered silicon nitride and contained 8 wt % yttria and 2 wt % alumina as the major sintering additives. RM 20 was found to be suitable for slip casting gas turbine engine components such as rotors and adiabatic diesel engine parts.

Flexural test specimens ($\sim$32 mm long by $\sim$6 mm wide by $\sim$3 mm thick) were machined from two billets, namely, A 42 and A 40. All faces were ground lengthwise using 320 grit diamond wheels; the edges were chamfered (lengthwise) to prevent notch effects.

For flexural strength evaluation, specimens were tested in $\frac{1}{4}$-point, 4-point bending (inner span is one-half of outer span) in an Instron testing machine (model 1125) using specially designed self-aligning ceramic fixtures[1] made from hot-pressed SiC. The outer and inner knife edges of the testing fixture were spaced 19 mm and 9·5 mm apart, respectively. The high temperature bend tests were conducted in air using a rapid temperature-response furnace attached to the testing machine head. In high temperature tests, specimens were held at the test temperature for 15 min to achieve equilibrium before testing was begun. No preload was applied on test specimens for either room temperature or high temperature tests. All specimens were tested at a machine crosshead speed of 0·5 mm min^{-1}.

The flexural stress rupture tests at elevated temperatures (800 to 1200°C) in air were also conducted in four-point bending using the self-aligning ceramic fixture and furnace. The load was applied to the test specimen through a cantilever arm deadweight assembly. The experimental set-up was equipped with a microswitch to cut-off power to the furnace and the timer at the instant failure of the specimen occurred. The total time-to-failure was recorded. An overall view of the test set-up is shown elsewhere.[2]

3 RESULTS AND DISCUSSION

3.1 Chemical composition and phases

Silicon nitride, containing various oxides such as MgO, Al_2O_3 and Y_2O_3 and prepared either by conventional hot-pressing or sintering methods, is extremely sensitive to chemical impurities or additives in influencing its mechanical strength properties. In general, all of these oxide additives help in promoting full densification of the bulk material. In particular, the addition of Al_2O_3 has a wide range of effects, namely, lowering sintering and hot-pressing temperatures and preventing or reducing oxidation at intermediate temperatures (600–1000°C). Some disadvantages include suppressing crystallization of the intergranular phase and promoting its presence as an amorphous phase, lowering of high-temperature fracture strength due to glass formation, or promoting subcritical crack growth and rapid oxidation above 1000°C. The effects of Al_2O_3 addition in silicon nitride powder are well discussed by Smith and Quackenbush.[3] RM 20 material primarily contained 8 wt% Y_2O_3 and 2 wt% Al_2O_3. X-ray diffraction patterns taken from the as-machined bulk samples of RM 20 revealed primarily β-Si_3N_4 and traces of the K-phase ($YSiO_2N$). In the absence of Al_2O_3 (or containing only small amounts of $\leq 1\%$), yttria-doped silicon nitride shows the presence of several secondary crystalline phases such as $Y_2Si_3O_3N_4$, $Y_4Si_2O_7N_2$ (J-phase), $Y_{10}Si_6O_{24}N_2$ (H-phase) and $YSiO_2N$ (K-phase). These crystalline phases are usually intergranularly dispersed in a β-Si_3N_4 matrix, and control particularly, the high temperature strength of the material. However, all of these phases are susceptible to oxidation with varying degrees of molar volume changes, thus degrading the material's strength as discussed by Smith and Quackenbush,[3] Lange,[4] Wills *et al.*[5] and Lange *et al.*[6]

3.2 Flexural strength vs temperature

At room temperature, ten specimens each from two billets, A42 and A40, respectively, were tested in four-point bending to determine the fast fracture strength. These billets were of identical composition but processed at different times. Typical statistical variation in fracture strength, σ_F, at 20°C for both billets is shown in Fig. 1. For billet A42, the σ_F varied from a minimum of 785 MPa to a maximum of 988 MPa with an average strength of 873 MPa, Weibull modulus of 13 and a standard deviation of 79 MPa. For billet A40, the σ_F varied from a minimum of 680 MPa to a maximum of 854 MPa with an average strength of 777 MPa, Weibull modulus of 16 and a standard deviation of 59 MPa. At 20°C, there is significant difference in σ_F

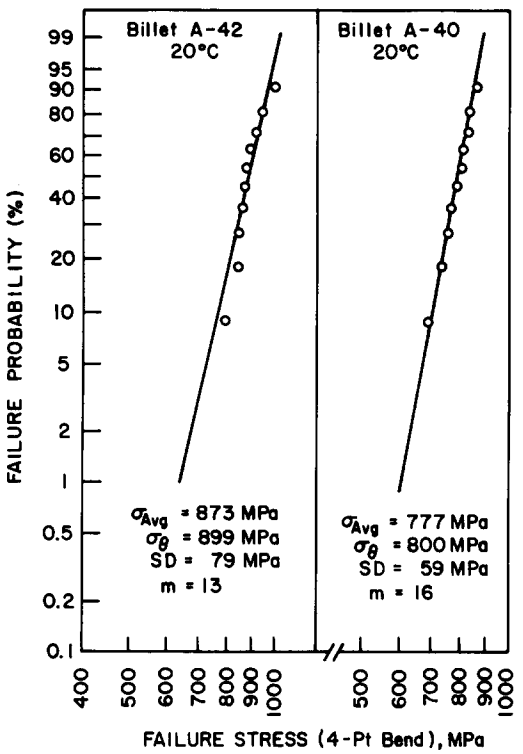

Fig. 1. Statistical variation in fracture strength at 20°C for yttria-doped sintered silicon nitride (Ford Material—RM 20).

for the two billets and, therefore, the two sets of data points are not combined and are shown separately, Fig. 1. Comparison of the σ_F values obtained at 20°C for the two billets indicates that billet A42 is stronger than billet A40. This difference in σ_F is primarily due to large variations in flaw sizes of the as-processed billets. The failure initiating flaws were of the same type (morphology) in both billets as seen later. Examination of the fracture surfaces revealed that all failures in specimens tested at 20°C were associated with porosity in the material. A typical failure occurring at a porous region in a specimen of billet A42 is shown in Fig. 2. These porous regions were approximately 50 μm wide and 100 μm deep (see Fig. 2) for billet A42 and slightly bigger in billet A40. Closer examination of the flaw site revealed that the grain morphology of β-Si_3N_4 inside the porous region appeared to be primarily needle shape (accicular), and less so away from it, see Fig. 2(b). The presence of such large porous regions suggests that full densification of the bulk material did not occur during sintering and an extended period of sintering might well reduce porosity. These flaws could very well be regarded and classified as pockets of unsintered or partially sintered material. In spite

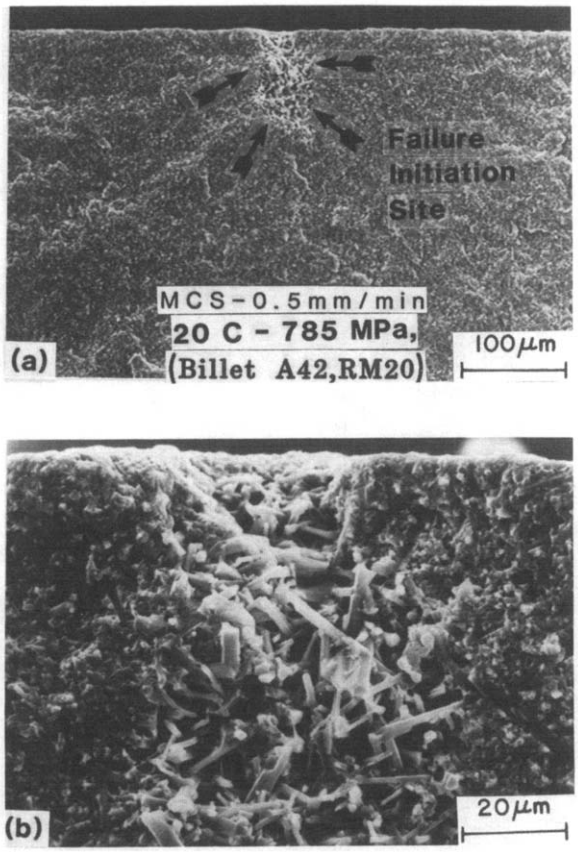

Fig. 2. Typical failure initiation site as seen in SEM for a specimen tested in fast fracture mode (machine crosshead speed = 0·5 mm min^{-1}). (a) Failure originated at the porous or partially sintered region. (b) Presence of β-silicon nitride needles inside the porous region.

of large variations in strength, it appears that the yttria/alumina-doped, sintered silicon nitride (Ford material, RM 20) can be fabricated to yield high strength material ($\geq$800 MPa) at 20°C and the strength can be significantly improved by optimizing sintering conditions.

Flexural strength was also evaluated at higher temperatures (400 to 1400°C), and the variation in strength as a function of temperature is shown in Fig. 3. In spite of the fact that these specimens were tested in fast fracture mode (machine cross-head speed = 0·5 mm min^{-1}), those specimens tested above 800°C showed minor surface color change (dark gray or black to whitish gray). Complete strength data and the failure sources are given in Table 1. Data show a large scatter due to variations in flaw size as noted at 20°C. In addition, large pores or pockets of partially sintered material become the preferential sites for low temperature oxidation as observed in

TABLE 1
Fast Fracture Strength Data for Yttria-Doped Sintered Silicon Nitride (Ford Material—RM 20)

Billet no.	*Test temp. (°C)*	*Fracture strength (MPa)*	*Failure origin, discoloration, oxidation, SCG, bending*
A 42	20	856	Porosity
A 42	20	851	Porosity
A 42	20	834	Porosity
A 42	20	834	Porosity
A 42	20	933	Porosity
A 42	20	904	Porosity
A 42	20	988	Porosity
A 42	20	863	Porosity
A 42	20	878	Porosity
A 42	20	785	Porosity, Fig. 2
A 40	20	823	Porosity
A 40	20	724	Porosity
A 40	20	821	Porosity
A 40	20	799	Porosity
A 40	20	854	Porosity
A 40	20	680	Porosity
A 40	20	795	Porosity
A 40	20	774	Porosity
A 40	20	755	Porosity
A 40	20	746	Porosity
A 42	400	821	Porosity
A 42	400	922	Porosity
A 40	400	792	Porosity
A 40	500	505	Porosity (200 μm wide & 250 μm deep), minor oxidation, Fig. 4
A 40	500	852	Porosity
A 40	500	840	Porosity
A 40	500	887	Porosity
A 40	600	686	Porosity, minor oxidation, Fig. 5
A 40	600	779	Porosity
A 40	600	878	Porosity
A 42	600	757	Porosity
A 42	600	788	Porosity
A 40	800	790	Porosity
A 40	800	653	Porosity
A 40	800	735	Porosity
A 42	800	713	Porosity
A 42	800	687	Porosity

TABLE 1—*contd.*

Billet no.	*Test temp. (°C)*	*Fracture strength (MPa)*	*Failure origin, discoloration, oxidation, SCG, bending*
A 42	1 000	609	Porosity and corner failure, minor discoloration
A 42	1 000	665	Porosity
A 40	1 000	634	Porosity and oxidation
A 40	1 000	724	Porosity
A 40	1 200	542	Porosity and oxidation
A 40	1 200	518	Porosity and oxidation
A 42	1 200	522	Porosity and oxidation, discoloration
A 42	1 200	604	Porosity and oxidation, discoloration
A 42	1 300	326	SCG region from corner, discoloration, oxidation
A 42	1 300	318	SCG region, discoloration, oxidation
A 42	1 300	303	SCG region from corner, discoloration, oxidation, specimen displayed slight bending, Fig. 6
A 42	1 400	560	Porosity, turned white, oxidation, no bending
A 42	1 400	220	Large region of oxidation and SCG, turned white, specimen displayed slight bending
A 42	1 400	202	Large region of oxidation and SCG, turned white, specimen displayed slight bending

As-processed material is dark gray or black.
SCG = Slow crack growth.

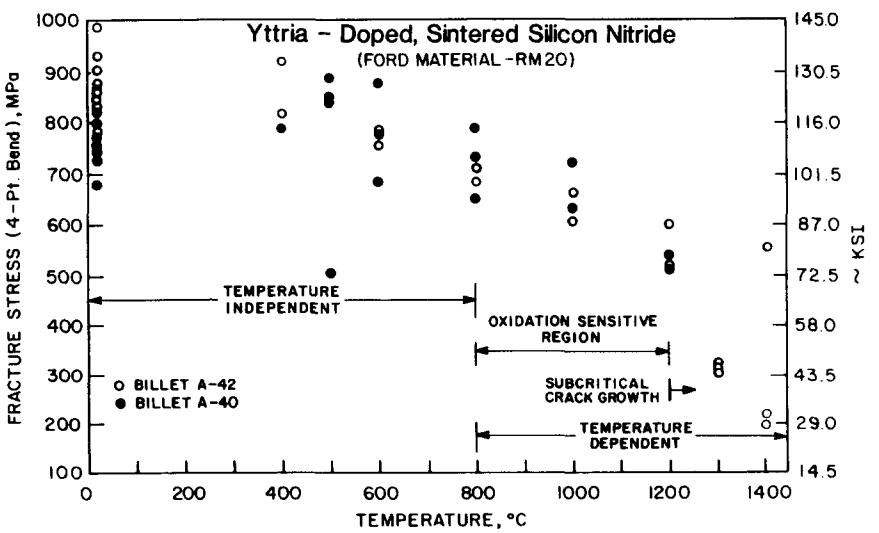

Fig. 3. Variation in fracture strength as a function of temperature.

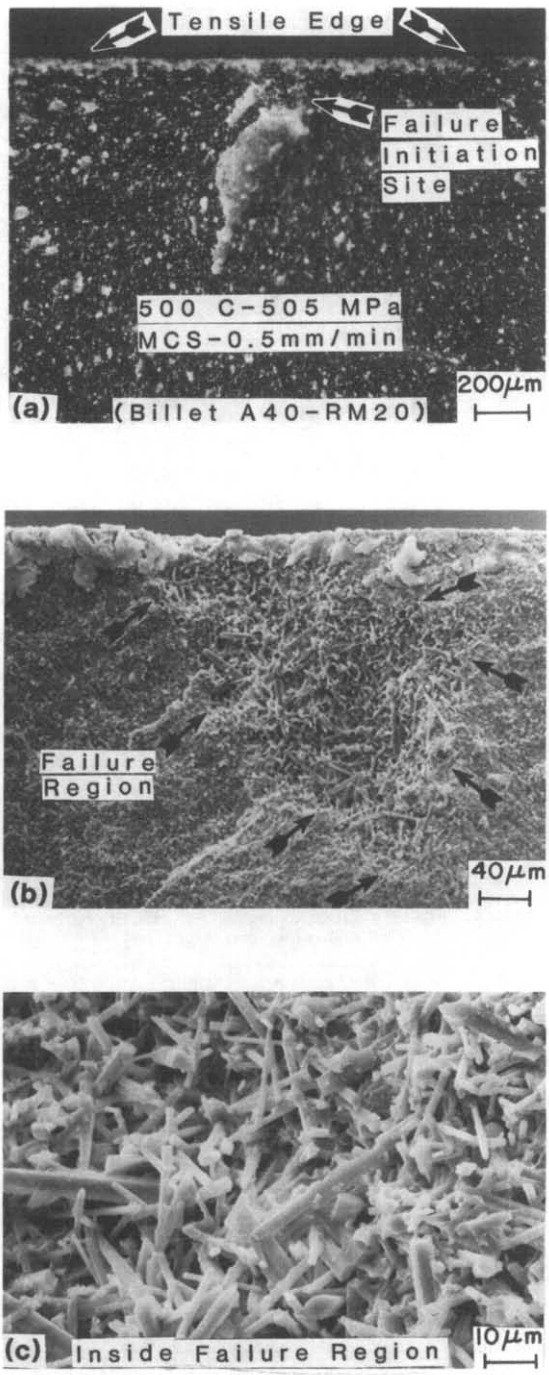

Fig. 4. Surface initiated failure occurring at a large porous or partially sintered region. (a) Fracture surface as seen in polarized light. (b-c) SEM fractographs of failure zone.

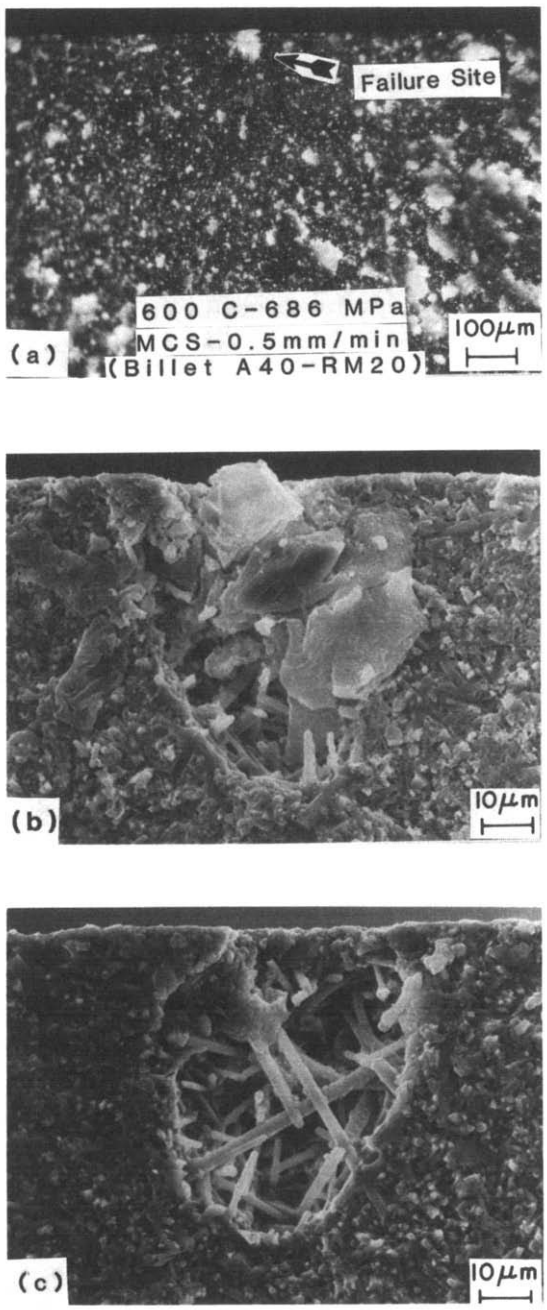

Fig. 5. Surface initiated failure at an oxidation pit. (a) Failure initiation site as seen in polarized light. (b) SEM fractograph of the failure site seen in (a) showing oxide flakes in the porous region. (c) SEM fractograph of the failure site seen on the other half of the test specimen.

tests made at 500 and 600°C. Preliminary static oxidation results did not show any significant weight gains at temperatures up to 800°C for periods of 100 h and, therefore, it is believed that oxidation did not play a major role in causing failures during fast fracture up to 800°C, provided the material did not contain unusually large pores susceptible to oxidation. It should be noted that four specimens of billet A40 were tested at 500°C, three failed at stresses above 800 MPa and one failed at 505 MPa due to a very large pocket of unsintered or partially sintered material, Fig. 4. Some signs of oxidation are visible along the edge, Fig. 4(a). Note the porous region is 200 μm wide and 250 μm deep. The grain morphology (Fig. 4(c)) is similar to that seen at 20°C. Even though the test temperatures of 500° and 600°C are relatively low temperatures for oxidation to occur in sintered silicon nitride, some evidence in the form of oxidation pits was visible both on the tensile surface and fracture surface. Typical failure occurring at a porous region, promoting local oxidation pit formation as the failure initiation site, at low temperatures such as 600°C is shown in Fig. 5. Examination of both fractured halves (Fig. 5(b) and (c)) show the corresponding failure initiation sites and the association of a large pore at the failure site. Note signs of oxidation, such as oxide flake formation taking place inside the pore, Fig. 5(b). Similar types of oxidation induced failure sites were observed at 1000°C and 1200°C, and a detailed description of the fracture morphology is given elsewhere.[7] It is believed that the decrease in strength, σ_F, (relative to σ_F at 20°C) in this temperature region (600 to 1200°C) is considerably influenced by the presence of large pores which promote rapid oxidation as supported by fractographic observations (Figs 4, 5) and stress rupture tests (see later). The load–deflection curves showed linear elastic behaviour indicating the absence of subcritical crack growth or glass formation as confirmed by the fracture surfaces.

At 1300°C and above, σ_F decreased abruptly, Fig. 3, and the fracture surface showed a localized slow crack growth (SCG) region as the failure zone, Fig. 6(a). The SCG region is distinct in its appearance, being characterized by a rough surface. The mode of fracture during SCG is primarily intergranular, Fig. 6(b), and outside the SCG region, it is a mixture of transgranular and intergranular crack propagation, Fig. 6(c). The load-deflection/time curve showed significant deviation from the elastic line, Fig. 6(d), indicative of creep deformation. Similar behavior was observed in tests made at 1400°C, except that the creep deformation was much more extensive. The grains were smeared due to viscous glass flow on the fracture face and the specimen showed slight bending.[7] At these high temperatures (1300–1400°C), the deformation behavior of this sintered silicon nitride (Ford Material-RM 20) is similar to that observed in another commercially available sintered silicon nitride (GTE-SNW 1000).[8,9]

Fig. 6. (a–c) SEM fractographs showing fracture at 1300°C. Slow crack growth (SCG) region originated from corner.

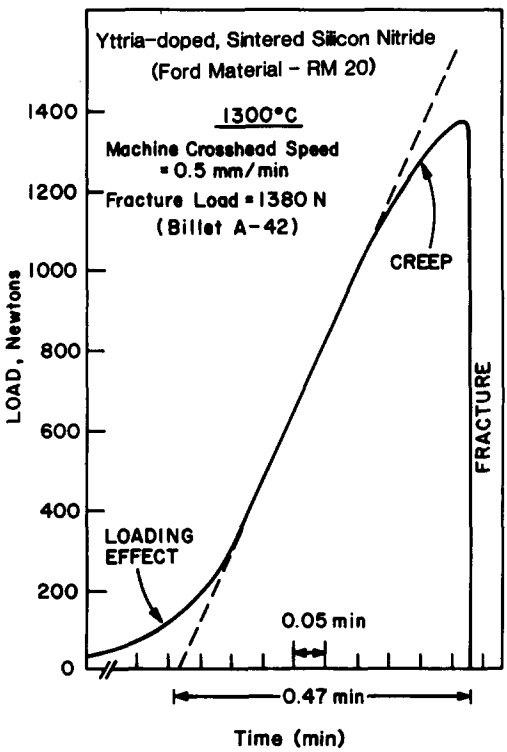

Fig. 6—*contd.* (d) Load-deflection curve showing creep deformation.

3.3 Flexural stress rupture

It should be pointed out that yttria-doped silicon nitride, consolidated by hot-pressing or sintering, has shown severe degradation of strength at intermediate temperatures (600 to 1000°C)[3,4,6,10–13] due to both static oxidation and stress enhanced oxidation. Therefore, flexural stress rupture tests were carried out as a function of temperature and applied stress, in order to determine (i) the materials susceptibility for low temperature instability, (ii) the presence of slow crack growth at high temperatures (1200 to 1400°C) and (iii) to identify allowable stress levels for limited time ($\leq$100 h) without showing any creep. A total of 22 specimens taken from both billets were tested in stress rupture mode and the results are summarized in Table 2. At 700°C, one specimen was tested at an applied stress level of 413 MPa and sustained the stress for over 200 h without showing any signs of bending and failure. At 800°C, test specimens sustained the applied stress of 276 and 344 MPa for over 200 h without showing failure and bending (creep) effects. At an increased stress of 413 MPa and 800°C, two specimens were tested, one survived over 300 h without showing any

TABLE 2
Flexural Stress Rupture Results for Yttria-Doped Sintered Silicon Nitride (Ford Material—RM 20)

Billet no.	*Test temp. (°C)*	*Applied stress (MPa)*	*Failure time (h)*	*Sustained time without failure (h)*	*Fracture origin, discoloration,[a] local oxidation region (LOR), spot formation, slow crack growth (SCG), specimen bending*
A 42	700	413	—	214	No discoloration, no spot formation, no bending
A 40	800	276	—	260	Color—whitish gray, no spot formation, no bending
A 40	800	344	—	220	Color—whitish gray, no spot formation, no bending
A 40	800	413	225	—	LOR, uniform oxidation, porosity, color—whitish gray, Fig. 7
A 42	800	413	—	336	Color—whitish gray, no spot formation, no bending
A 42	800	482	88	—	LOR, color—gray, no spot formation, no bending
A 40	1 000	344	—	213	Color—white, no spot formation, no bending
A 40	1 000	344	—	313	Color—white, no spot formation, no bending
A 42	1 000	344	35	—	LOR, uniform oxidation, color—white, no spot formation, no bending, Fig. 8
A 42	1 000	344	—	306	Color—white, no spot formation, no bending
A 42	1 000	413	1	—	Porosity & oxidation, uniform oxidation, color—whitish gray, no bending, Fig. 9
A 42	1 000	413	6·4	—	LOR, uniform oxidation, color—white, no bending, Fig. 8
A 42	1 000	413	15	—	LOR, uniform oxidation, color—white, no bending
A 42	1 000	413	—	309	Color—white, no spot formation, no bending
A 42	1 000	482	0·3	—	Surface porosity, color—whitish gray, no spot formation, no bending
A 42	1 000	482	0·5	—	Surface porosity, color—whitish gray, no spot formation, no bending
A 42	1 000	482	12·5	—	Surface porosity, color—white, uniform oxidation, no bending
A 42	1 000	482	24	—	LOR, uniform oxidation, color—white, no spot formation, no bending
A 42	1 100	413	—	210	Minor discoloration, specimen displayed slight bending
A 42	1 200	413	0·1	—	LOR around corner, no discoloration, no bending, Fig. 10
A 42	1 200	413	—	258	Minor discoloration, specimen displayed bending
A 42	1 200	482	0	—	Failed instantly at a large β-Si_3N_4 needle, no oxidation, no bending

[a] As-processed material is dark gray or black.

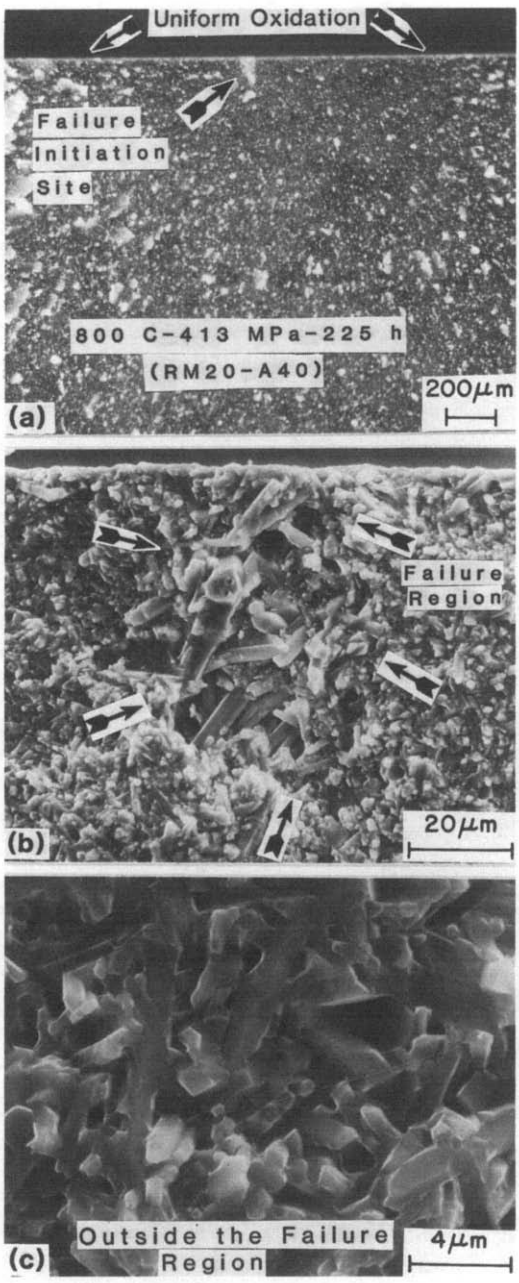

Fig. 7. Typical failure initiation site seen in a stress rupture specimen at 800°C. (a) Fracture surface seen in polarized light. Note the presence of uniform oxidation along the tensile edge. (b) SEM fractograph showing the failure initiation site (oxidation pit) seen in (a) consists of a porous region. (c) SEM fractograph taken in a region away from the failure site showing random porosity distribution and grain morphology. Failure mode appears to be primarily transgranular.

signs of bending and the other one failed after 225 h. Examination of the fracture surface of the failed specimen revealed the failure initiation site as a local oxidation region (LOR), Fig. 7, associated with porosity and uniform oxidation all along the tensile edge. However, at an increased stress of 482 MPa, the specimen failed after 88 h and the fracture surface showed a porosity-associated oxidation region.[7] Away from the fracture origin, the fracture surface showed the smooth appearance of crack propagation indicating transgranular fracture, Fig. 7. Up to 800°C, it is believed that oxidation did not play a significant role in causing failures for two reasons: (i) No significant weight gains were observed among those specimens which survived over 200 h. (ii) Fracture surfaces did not reveal penetration of localized or preferential oxygen diffusion areas which would suggest oxide related failures. However, it should be pointed out that the presence of large pores promotes oxidation and these become preferential sites for oxidation to occur, and this may be a good reason to observe oxidation-related failures in fast fracture (Fig. 4) at low temperatures such as 500 and 600°C, Figs 4 and 5, respectively, as discussed earlier. The specimen which sustained 336 h without failure showed that the material (RM 20) is capable of sustaining high stress levels provided that processing and fabrication flaws can be controlled.

At 1000°C, the material showed a distinctly different behaviour than that seen at 800°C. At a low stress level of 344 MPa, four specimens were tested; three survived over 200 h without showing bending and failure and one failed in 35 h, Fig. 8. Examination of the fracture surface revealed a uniform oxidation layer (approximate thickness 60 μm) and a local failure initiation site faintly visible (Fig. 8) and associated with fine porosity distribution. The X-ray diffraction pattern taken from the surface of the oxidized specimen (which survived 306 h) revealed the identity of the oxide as $Y_2Si_2O_7$. As the applied stress was increased to 413 MPa, the time-to-failure decreased significantly as displayed by three out of four specimens which failed in 1, 6·4 and 15 h, respectively. Examination of the fracture surfaces for all three specimens revealed either an oxidation pit or a small local oxidation region, Fig. 8 and Fig. 9. The failure initiation site and the associated porosity for the specimen failing after 1 h is shown in Fig. 9. The rapid failure of the specimen was primarily due to the presence of a large pore (20–40 μm wide and 80 to 110 μm long) or a pocket of partially sintered material, Fig. 9(b), similar to that seen earlier. Note the thickness of the uniform oxidation layer is about 15 to 20 μm. The specimen which sustained the applied stress for over 300 h (Table 2) without showing any signs of bending and failure, shows that the sintered material is capable of sustaining these stress levels provided that processing and fabrication flaws are controlled. At high stress levels of 482 MPa, failure occurred rapidly within 0·3 to 24 h. It is important to point

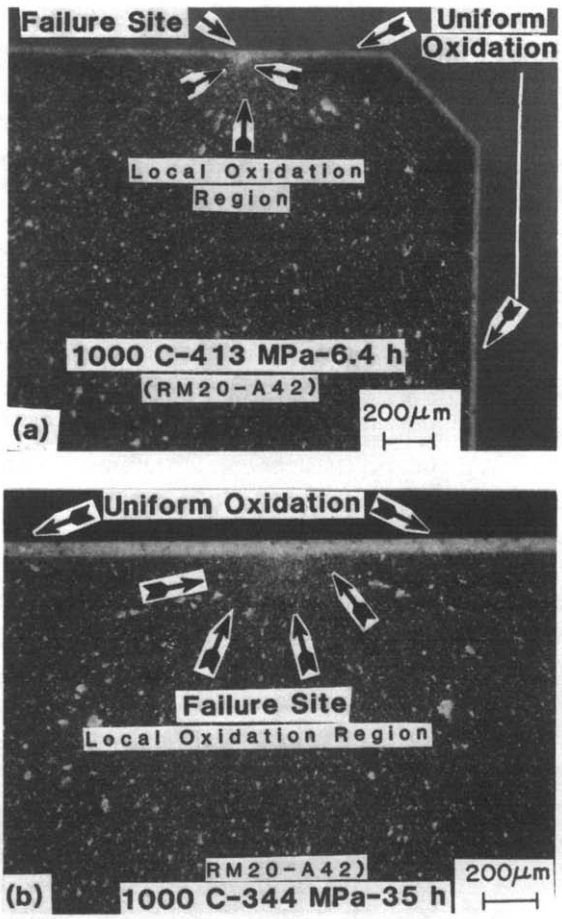

Fig. 8. Typical failure initiation sites seen in stress rupture specimen at 1000°C. Micrographs taken in polarized light. Note the presence of uniform oxidation, and localized oxidation region as the failure site.

out that in spite of the fact that failures occurring at 800 and 1000°C were time-dependent (see Table 2), fracture surfaces of these specimens did not show clearly the presence of slow crack growth similar to that seen in tests made at 1300°C or above (Fig. 6).

At 1100°C and above, the RM 20 material showed distinctly different stress rupture behavior than that seen at temperatures below 1000°C. At 413 MPa and 1100°C, the material was able to withstand the stress for periods over 200 h without showing failure or degradation in strength. However, careful examination of the specimen revealed slight bending,[7] suggesting the onset of viscous flow, due to residual glass softening. At 1200°C, two specimens were tested at applied stress of 413 MPa, one failed in

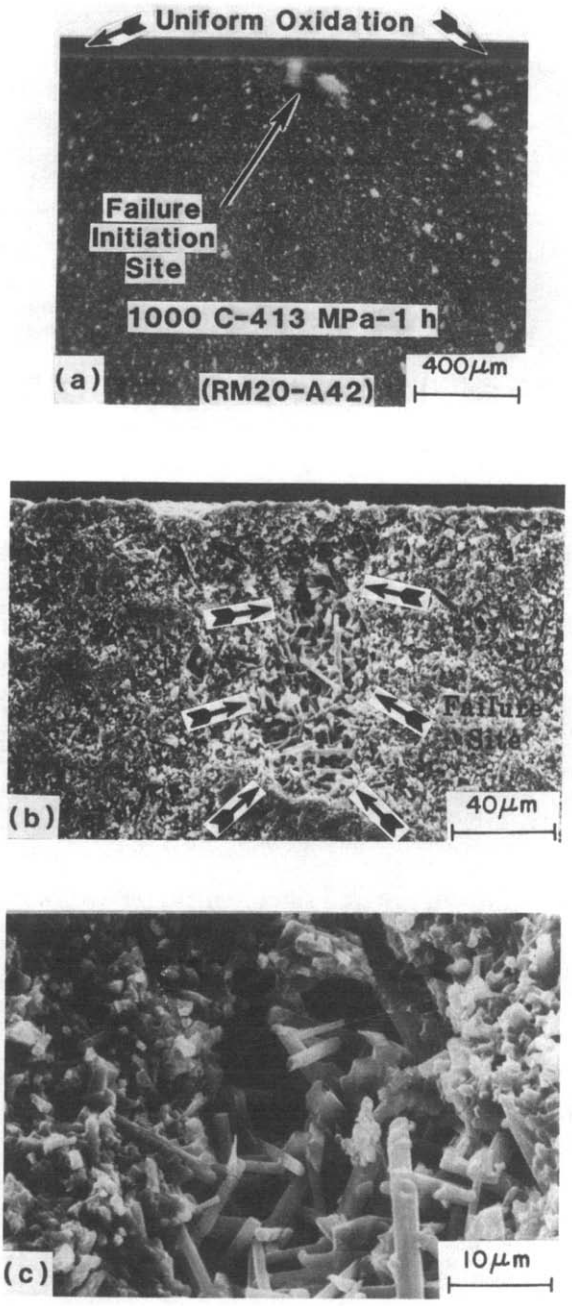

Fig. 9. Typical failure site seen at 1000°C. (a) Polarized light. (b–c) SEM fractographs.

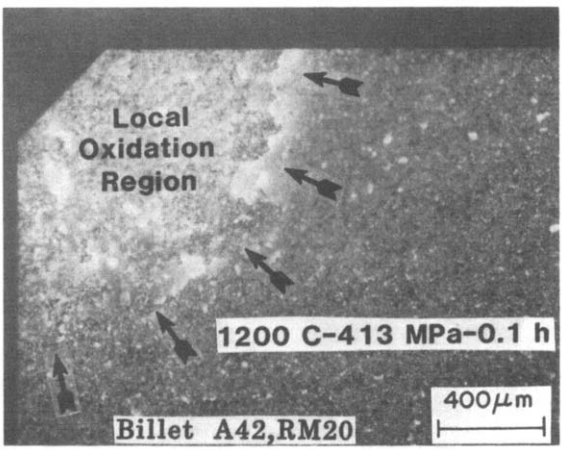

Fig. 10. Fracture surface seen in polarized light showing corner related oxidation region in a stress rupture specimen at 1200°C.

0·1 h, due to the combined effects of oxidation and slow crack growth (Fig. 10), and the other specimen sustained 258 h without failure but showed bending. As the applied stress was increased to 482 MPa, failure occurred instantly. This slight (microscopic) bending of specimens clearly points out the importance of this temperature and applied stress (1100°C and 413 MPa) for the onset of grain-boundary sliding as a creep mechanism.

4 CONCLUSION

The yttria/alumina-doped, sintered silicon nitride (Ford Material—RM 20) of moderate strength ($\sim$800 MPa) as developed showed significant variations in strength at 20°C due to large variations in processing flaw size (or pockets of partially sintered material). The strength appears to be independent of temperature, up to 800°C. The strength decreases slowly as a function of increasing temperature up to 1200°C. The material is sensitive to oxidation in this temperature region. Above 1200°C, degradation in strength occurs due to both oxidation and viscous flow of the glassy phase or grain-boundary sliding.

Flexural stress rupture testing at 800°C and 1000°C indicated that the material can sustain 344 MPa and 276 MPa without failure, for a limited time ($\leq$100 h), respectively. Above 1000°C, the material is unstable and shows both oxidation and creep deformation which makes it unsuitable for use as a rotor in a gas turbine. However, it could be used for diesel engine applications.

ACKNOWLEDGEMENTS

The author is grateful to A. Ezis and W. Copple for making and supplying the material, to E. Stiles and H. Blair for X-ray diffraction, and R. Goss for SEM work. Thanks are due to the Department of Energy and NASA for partly supporting the work under contract numbers DAAG-46-77-C-0028 and DEN 3-167.

REFERENCES

1. Govila R. K., Ceramic life prediction parameters, *Tech. Report, AMMRC, TR 80-18*, Army Materials and Mechanics Research Center, Watertown, Mass., USA, May 1980.
2. Govila, R. K., Flexural stress rupture strength of sintered alpha SiC, in *Time-Dependent Failure Mechanisms and Assessment Methodologies*. Eds J. G. Early, T. R. Shives and J. H. Smith, Cambridge University Press, New York, 1983, 100–10.
3. Smith, J. T. and Quackenbush, C. L., 'Phase effects in Si_3N_4 containing Y_2O_3 or CeO_2: I, Strength; II, Oxidation, *Am. Ceram. Soc. Bull.*, **59** (1980) 529–37.
4. Lange, F. F., Fabrication and properties of dense polyphase silicon nitride, *Am. Ceram. Soc. Bull.*, **62** (1983) 1369–74.
5. Wills, R. R., Holmquist, S., Wimmer, J. M. and Cunningham, J. A., Phase relationships in the system Si_3N_4—Y_2O_3—SiO_2, *J. Mater. Sci.*, **11** (1976) 1305–9.
6. Lange, F. F., Singhal, S. C. and Kuznicki, R. C., Phase relations and stability studies in the Si_3N_4—SiO_3—Y_2O_3 pseudoternary system, *J. Am. Ceram. Soc.*, **60** (1977) 249–52.
7. Govila, R. K., Strength characterization of yttria-doped, sintered reaction bonded silicon nitride, *Tech. Rept. No. SR-86-36*, Ford Motor Company, Dearborn, USA, March 1986.
8. Quackenbush, C. L. and Smith, J. T., GTE sintered silicon nitride, *ASME Paper 84-GT-228*, American Society of Mechanical Engineers, New York, Sept. 1984.
9. Govila, R. K., Strength characterization of yttria-doped sintered silicon nitride, *J. Mater. Sci.*, **20** (1985) 4345–53.
10. Tighe, N. J., Kuroda, K., Mitchel, T. E. and Heuer, A. H., In-situ oxidation of Y_2O_3-doped Si_3N_4, in *Electron Microscopy 1980, Vol. 4, High Voltage*, Eds P. Brederoo and J. Van Landuyt, North-Holland Publishing Company, New York, 1980, 310–13.
11. Benn, K. W. and Carruthers, W. D., 3500 Hour durability testing of commercial ceramic materials, *Third Quarterly Progress Rept., Air Res. Manuf. Comp. of Arizona*, NASA contract DEN 3-27, Sept.–Nov. 1978.
12. Govila, R. K., Mangels, J. A. and Baer, J. R., Fracture of yttria-doped, sintered reaction-bonded silicon nitride, *J. Am. Ceram. Soc.*, **68** (1985) 413–18.
13. Govila, R. K., Fracture and intermediate temperature instability in yttria-doped hot-pressed silicon nitrides, *Am. Ceram. Soc. Bull.*, **65** (1986) 1287–92.

Received 12 December 1986; revised version received 15 July 1987; accepted 24 July 1987